Stratified Sampling Based Compressed Sensing for Structured Signals

Theresa Loss, Matthew J. Colbrook , and Anders C. Hansen

***Abstract*—Structured compressed sensing takes signal structure into account and thereby outperforms earlier compressed sensing methods. However, results are usually based on sampling in the Fourier domain, such as in Magnetic Resonance Imaging. In the time domain, the benefits of structured compressed sensing are still unknown. This paper introduces concepts that incorporate the signal structure into both the acquisition and reconstruction of compressed sensing in time and image domain applications. First, a stratified-random sampling pattern is proposed to improve the recovery of the dominant low-frequency range of natural signals. A *decay of primes* criterion is developed to evaluate the properties of the sensing matrix and is used to optimize the sampling pattern. Second, the sparsity of the Fourier transform as the representation domain is improved by estimating the signal structure in a preprocessing step, and then adapting the grid of the Fourier transform. In contrast to existing methods, *grid stretching* is integrated into the fast Fourier transform to reduce computational complexity. Both structured acquisition and reconstruction are evaluated using simulations, as well as two real-world applications: wireless sensor networks in structural health monitoring and electron microscopy. Results show that both reconstruction errors and robustness can significantly be improved by incorporating structure into the acquisition and reconstruction. Our approach highlights the importance of structure in time- and image-based sensing applications and aims to trigger subsequent research on the relevant mathematical background and applications to engineering fields.**

***Index Terms*—Structured compressed sensing, stratified random sampling, electron microscopy, structural health monitoring**

I. Introduction

TECHNOLOGICAL advances in physical and biological sensing applications frequently result from the need to overcome a restriction on the number of measurements taken by the system. This may result from a limited power supply as present in wireless sensor networks [1], limited measurement time such as the duration of examination in Magnetic Resonance Imaging (MRI) [2], as well as restrictions in energy dose on the subject in Electron Microscopy (EM) [3].

Apart from tackling the problem from the hardware side, signal processing methods can be applied to reconstruct measurements from far fewer samples then the Nyquist criterion suggests. By exploiting the sparseness of the original signal, compressed sensing (CS) has successfully been used in the last 15 years to solve the underdetermined inverse problem of reconstruction in many applications [4]–[7]. Recently, artificial intelligence has also been used in sampling problems, with neural networks (NNs) trained to optimally reconstruct original signals from a limited number of measurements [8], [9]. However, there are currently three drawbacks of this data-based approach which should not be neglected:

1. The optimal trade-off between stability and accuracy of NNs is mostly unexplored [10], and there is evidence that many current AI technologies may be unstable [11]–[17]. For example, it has been shown that tiny perturbations or structural changes in the image signal can lead to major changes in NN reconstruction [16].
2. The problem of false negatives is important in clinical practice. For example, Facebook and NYU's 2019 FastMRI challenge reported that networks that performed well in terms of standard image quality metrics were prone to false negatives and failing to reconstruct small, but physically relevant image abnormalities [18]. The 2020 version of the challenge subsequently focused on pathologies, noting the problem of *AI-generated hallucinations* [19].
3. Reconstruction accuracy of a trained NN does not necessarily increase (and may in fact decrease) with an increased subsampling ratio. Typically, NNs need to be trained separately for varying subsampling ratios [16] (and on large training sets), which is computationally very expensive.

These considerations are essential in medical and structural diagnosis since inaccuracies in the measurement system can mask or generate crucial events in the output signal. Therefore, we focus on so-called structured CS, which takes the signal's sparse structure into account in both acquisition of measurements and reconstruction of the original signal to increase compression rates and robustness [20], [21].

Despite the success of structured CS [22]–[28], including an abundance of elaborated theory, examples and applications are mainly restricted to sensing conducted in the Fourier domain, such as radio frequencies in MRI [29]. In applications where measurements are conducted in the time or image domain, i.e. subsampling from a time series with equidistant samples or subsampling from an image with defined location of pixels, there is a lack of CS-based strategies on how to incorporate structure into acquisition reconstruction of measurements.

This work aims at bridging the gap between state-of-the-art methods in compressed sensing and their application to sensing in the time or image domain. Analogous to MRI, in which structured sampling was implemented first and mathematical proofs delivered subsequently, we follow an engineering approach and focus on establishing structured CS in time- and image-domain-based sensing applications. Results

Corresponding author: Theresa Loss.

T. Loss is with the Institute of Electrical Measurement and Sensor Systems, Graz University of Technology (e-mail: loss.theresa@web.de).

M.J. Colbrook and A.C. Hansen are with the Department of Applied Mathematics and Theoretical Physics, University of Cambridge (e-mail: m.colbrook@damtp.cam.ac.uk, ach70@cam.ac.uk).

Code is available upon request from T. Loss.

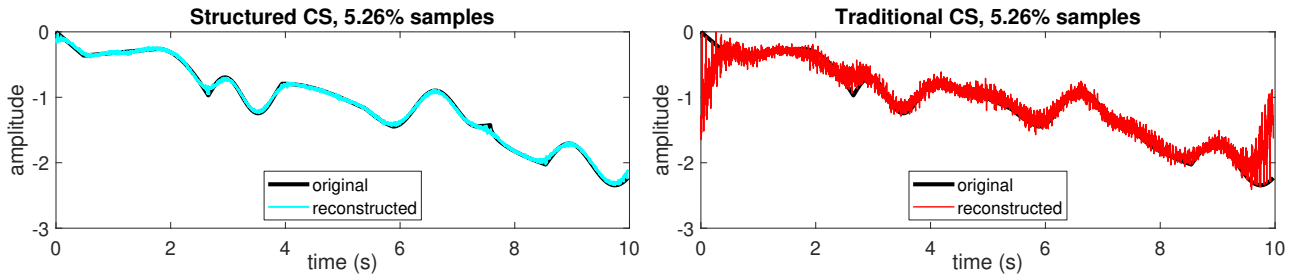

Fig. 1: Comparison of reconstruction results for the proposed method ("Structured" CS) and state-of-the-art CS ("Traditional" CS). Reconstruction from 5.26% of samples for a piecewise linear function with sampling for both methods in the time domain and reconstruction via the Fourier transform. Traditional CS uses uniform at random sampling in the time domain, whereas Structured CS uses structured sampling in the time domain and reconstruction via an adapted Fourier transform. Methods are presented in detail in the remainder of this paper (this example uses the model in §II-A with $N = 4000$.)

are demonstrated by means of two applications, namely electron microscopy (EM) and the relatively new field of structural health monitoring (SHM). However, methods are not limited to those fields and shall provide benefits for time- and image-domain-based sensing in many applications.

A. Structure in Acquisition

Signals can exhibit structure in several domains such as sharp localized edges in an image or distinct frequencies in the Fourier domain. Therefore, the structure needs to be considered during both acquisition and reconstruction. In this paper, we point in both directions and show the relevance of structure in time- and image-domain-based sensing.

Randomness of the sensing matrix has been one of the main principles during early CS approaches. However, and inevitably, structure in sensing matrices had to be explored when trying to implement the sensing matrices in real-world applications such as sensors and imaging hardware [30]. Hardware restrictions concerning storage limitations for random matrices and restriction of random acquisition have led to various implementations such as the random demodulator, the modulated wideband converter and random filtering [5]. Simultaneously, advances in mathematical theory have shown by the so-called flip test that signal structure needs to be incorporated into the sensing matrix to achieve optimal results [20]. The introduction of structured block-based acquisition has enabled the implementation of sensing matrices into sampling devices. Nevertheless, results are usually based on Fourier measurements [21].

To our knowledge, structured sensing has not yet been applied to the acquisition of either single samples in the time domain or single locations in an image. When reducing the number of measurements, ideal randomness cannot be guaranteed. By establishing criteria for the design of optimal time- and image-domain-based sensing, artefacts during reconstruction can be reduced. Additionally, real-world implementation of sensing matrices can be evaluated by using such criteria.

B. Structure in Reconstruction

The structure of the original signal needs to be incorporated into reconstruction methods to achieve optimal results. It is important to note that even though a signal might be sparse in an ideal representation basis, exactly determining that basis may be infeasible in practice. The difference between the ideal and the implemented representation basis, called *grid mismatch*, can never be fully resolved since any fixed discrete grid can not exactly match the physical parameters [31]. Several approaches have been suggested for resolving grid mismatch such as dictionary parameter learning and sparse signal estimation [32], dictionary learning with a restriction on grid size [33], and bias correction estimation [34].

In our approach, we aim to reduce grid mismatch by aligning the grid to the pre-estimated signal structure. By using efficient implementations of the representation domain, computation times shall be kept to a minimum while grid mismatch is reduced and reconstruction accuracy is optimized.

C. Relevance

Our approach's relevance is demonstrated through two exemplary applications using time- and image-domain-based sensing and reconstruction via the Fourier transform. First, our approach is applied to the emerging field of SHM, in which the condition of civil structures is frequently determined by means of wireless sensor networks. Since those sensors are often energy self-sufficient, CS is promising for reducing the energy for measurements and data transfer [35]–[37].

Second, we demonstrate the benefits of our results in the field of EM, which is used for imaging of fine-scale structures such as organic tissues and nanofibres [38], [39]. Since high-density sampling is needed to achieve high signal-to-noise ratios (SNR) but increases the risk of damage to the sensitive structures at the same time [40], CS holds high potential for reducing the number of electrons and improving the SNR.

A demonstration of results shows a significant improvement in reconstruction for structured CS (see Figure 1).

The remainder of this paper is organized as follows. §II presents the problem statement, including a brief introduction on CS theory and our signal model. §III includes the main results for structure-based sensing and structure-based reconstruction. Benefits of our approach are demonstrated in §IV by applying methods to real data of SHM and of EM imaging. §V summarizes results and relevance of proposed methods.

II. Problem Statement

A. Background

Following, for example, [41], we consider the following standard setup in CS. The original vector $x \in \mathbb{C}^N$ is acquired in a compressed form, $y \in \mathbb{C}^M$, via multiplication with the so-called *sensing matrix* $\Phi \in \mathbb{C}^{M\times N}$, $y = \Phi x$. Here, $M \ll N$. We assume that the measurement vector x is sparse in a representation domain corresponding to the matrix $\Psi \in \mathbb{C}^{N\times N}$ (so that $X = \Psi x$ is approximately sparse). If the measurement matrix Φ and the sparse representation Ψ are *incoherent* [41], then under suitable sparsity conditions, x can be recovered by solving standard l_1-regularization problems such as

$$\text{argmin}_{\tilde{x}\in\mathbb{C}^n} \|\Psi\tilde{x}\|_1 \quad \text{s.t.} \quad y = \Phi\tilde{x}, \tag{1}$$

$$\text{argmin}_{\tilde{x}\in\mathbb{C}^n} \|\Psi\tilde{x}\|_1 \quad \text{s.t.} \quad \|y - \Phi\tilde{x}\|_2 \leq \epsilon, \tag{2}$$

the latter being used in the presence of noise. In certain applications, such as MRI and the DFT, one must consider local coherences and structured compressed sensing [20].

In our approach, we focus on the acquisition of measurements in the time or image domain and on sparse representation via the Fourier transform. Throughout, Ψ is taken to be the DFT so that

$$(\Psi x)[k] = X[k] = \sum_{n=0}^{N-1} x[n] e^{\frac{2\pi i n k}{N}}, \tag{3}$$

for $k = 1, ..., N$ (see also §III-B for suitable adaptations). The sensing matrix Φ is taken to be the orthogonal projection onto $\text{span}\{e_j\}_{j\in\Omega}$ for some $\Omega \subset \{0, ..., N-1\}$ with $|\Omega| = M$. The set Ω is usually selected uniformly at random in CS, however, our approach introduces structured CS for the selection of Ω. Given an index set I, we let P_I denote the orthogonal projection onto the linear span of basis vectors indexed by I.

B. Signal Model

In physical and biological sensing applications, many signals exhibit significant structure and are dominated by the low frequency range. Considering our two exemplary applications, we find that a sensor in an SHM application will typically measure the fundamental frequency of an oscillation and multiples thereof, complemented by the structure's eigenfrequencies. Also, EM images of materials and biological tissues exhibit significant regularities as modeled in Figure 2.

We use $\mathcal{S}$ to denote the indices corresponding to non-zero components of X. Our model assumption is that the signal X is sparse (or approximately sparse) for frequencies $k > K$ and some positive K (i.e. dominated by the low-frequency range). This signal model exhibits a clear structure, and it is beneficial to take this into account in CS methods:

Structured signals need structured compressed sensing.

The importance of structure in CS has been demonstrated in MRI sensing, where structured acquisition has significantly improved reconstruction results [20]. Consequently, we examine the following question:

Is sampling uniformly at random optimal for reconstruction of structured signals at low sampling rates?

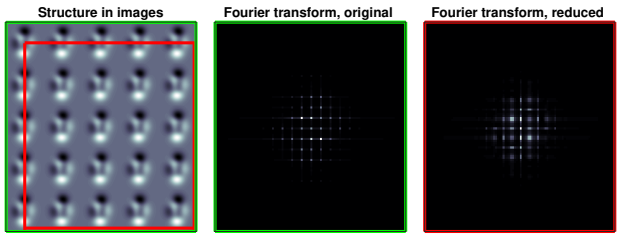

Fig. 2: Exemplary structure of electron microscopy images in image (left) and Fourier domain (middle, right). A magnified section of the sparse Fourier coefficients of the original image (middle) and a section of the image (right) is displayed.

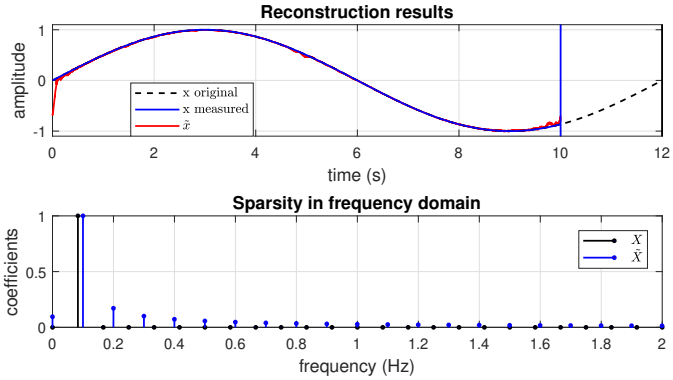

Fig. 3: Impact of window mismatch in the time domain (top) on the sparsity of Fourier coefficients (bottom). Reconstruction results are shown for a fundamental frequency of $0.083\,\text{Hz}$ in the case of window mismatch for a measurement period of $10\,\text{s}$. $\tilde{x}$ denotes the solution of the optimization problem in Equation (1) and $\tilde{X}$ denotes the frequencies $\Psi\tilde{x}$.

C. Structure in Acquisition

Unlike in the case of sensing in the Fourier domain, mathematical principles on structured sampling in time- and image-domain-based sensing problems have, to our knowledge, not yet been developed. Since low frequencies dominate the signals in both applications, the following questions should be addressed when designing the sensing matrix:

- What properties of the sensing matrix in the time and image domain are related to capturing a certain frequency?
- How can we ensure that the dominant lower frequencies in the signal are always captured?
- What properties does the sensing matrix need to fulfill to allow for robust reconstruction?

Our answers in §III-A to these questions are used to improve the design of the sensing matrix for a structured input signal.

D. Structure in Reconstruction

Additionally, the signal structure plays a major role in the reconstruction of real-world discrete measurement signals. When using the DFT as representation domain Ψ, the fast Fourier transform (FFT) is widely used to rapidly compute the Fourier transform of the discrete input signal. This leads to two major implications:

First, measurement devices are limited in terms of time and memory, and only capture a section of the original signal, which leads to discontinuities. Simultaneously, the FFT assumes periodic continuation of the input signal, which may lead to a mismatch between the measurement window and the signal structure (see Figure 3, top). Second, *window mismatch* also implies *grid mismatch*. The resolution R of the signal is defined by the measurement window T with $R = 1/T$, $T = t_N - t_1$ and t_n being the measurement time of samples $n \in \{1, ..., N\}$. Hence, the alignment of the equally spaced frequency grid of the DFT to the signal structure depends on the measurement window as shown in Figure 2 and Figure 3 (bottom). A refinement of the discretization can help to align the signal structure to the grid. However, the resulting interpolation of the Fourier coefficients leads to decreased sparsity and should be avoided.

Therefore, we aim to incorporate the signal structure into reconstruction by answering the following questions:

- How can the structure of the signal be estimated from compressed measurements?
- How can window and grid mismatch be addressed?
- What adaptions can be made to the FFT to increase reconstruction accuracy while keeping computational costs low?

Our answers in §III-B to these questions are used to optimize the sparse representation Ψ and improve reconstruction.

III. Main Results

This section contains the main results on incorporating the signal structure into the design of the sampling matrix during acquisition (§III-A) and into the sparsifying transform during the reconstruction of the signal (§III-B).

A. Sampling Algorithm

Structured sampling is well understood when sensing in the Fourier domain. However, this knowledge has not yet been transferred to time- and image-domain-based sensing. In the following, we design a sampling algorithm that takes the structure of signals into account in those sensing applications.

1) Motivation: The naive sampling approach would be to use uniform sampling with the sampling frequency f_s exceeding the highest dominant frequency $f_i = K$ in the spectrum by at least twice for exact recovery ($f_s \geq 2f_i$) [42]. Suppose that $a = N/(2K) \in \mathbb{Z}$ and that we select every ath sample (so that $\Omega = \{lN/(2K) : l = 0, ..., 2K-1\}$). Consider two signals x_1 and x_2 such that the corresponding X_1 and X_2 have $X_j[k] = 0$ if $k \neq i_j$ and $i_1 = r$, $i_2 = 2K + r$ ($0 \leq r < K$) with $X_1[i_1] = X_2[i_2]$. It follows from a straightforward calculation that $y_1 = y_2$ and consequently reconstruction of compressed measurements fails.

This well-known problem is overcome to some degree by using uniform at random (UAR) sampling (as practiced in Fourier sensing). However, in this case, we do not have any control over the distribution of the samples. If we reduce the number of samples down to the number of samples suggested by Nyquist, this may lead to large distances between any two samples. The following experiment shows the effect of large sample distances on the reconstruction error. An input signal is created by using the inverse DFT of a randomly selected frequency $k \leq K$. CS is then simulated by UAR sampling. When creating artificial gaps in the resulting UAR pattern, the reconstruction error increases significantly as soon as the maximum sampling distance exceeds a full period of the input signal (see Figure 4). Therefore, the combination of UAR sampling and the Nyquist criterion suggests *stratified random* (SR) sampling as defined below.

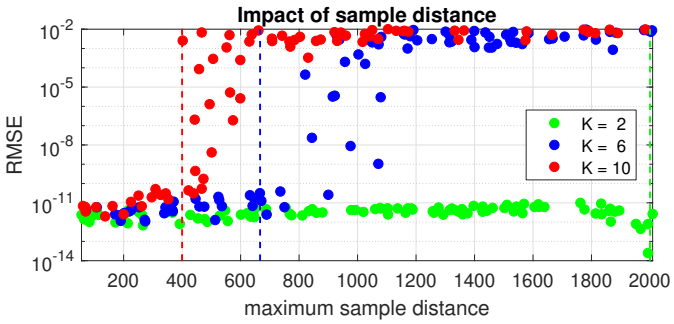

Fig. 4: Reconstruction errors for simulated gaps in the UAR sampling pattern. The signal is simulated for a randomly selected frequency $k \leq K$ for $K = 2, 6, 10$. Vertical lines represent one period of the input signal of length N/K. The signal length is $N = 4000$ and 100 runs are simulated. Root-mean-square errors (RMSE) displayed.

2) Stratified Sampling: Since our signal model is dominated by the low-frequency range, we focus on the recovery of those frequencies. We propose a *stratified* sampling pattern, in which the distance between adjacent samples is restricted. To introduce this, we first discuss multilevel sampling.

Definition 1 (Multilevel subsampling [20])**.** *Let* $\mathbf{N} = (N_1, \dots, N_l) \in \mathbb{Z}^l_{\geq 0}$*, where* $0 \leq N_1 < \cdots < N_l = N - 1$ *and* $\mathbf{m} = (m_1, \dots, m_l) \in \mathbb{N}^l$ *with* $m_k \leq N_k - N_{k-1}$ *for* $k = 1, \dots, l$*, and* $N_0 = 0$*. For each* $k = 1, \dots, l$*, let* $\mathcal{I}_k \subset \{N_{k-1} + 1, \dots, N_k\}$ *with* $|\mathcal{I}_k| = m_k$*. We refer to* $\mathcal{I}_1 \cup \cdots \cup \mathcal{I}_l$ *as an* $(\mathbf{N}, \mathbf{m})$*-multilevel subsampling scheme.*

For equidistant batch length L_B and a fixed number of samples m per batch, we introduce stratified subsampling.

Definition 2 (Stratified subsampling)**.** *Let* $\lambda > 0$*,* $L_B(K, \lambda) = \lceil N/(2K\lambda) \rceil$ *(batch length) and* $l = \lceil N/L_B(K, \lambda) \rceil$ *(number of batches). For* $k = 1, ..., l-1$*, set* $N_k = k \cdot L_B(K, \lambda) - 1$ *and set* $N_l = N - 1$*. If* $m_1 = m_2 = ... = m_l = m > 0$*, we refer to an* $(\mathbf{N}, \mathbf{m})$*-multilevel subsampling scheme as a stratified subsampling scheme. We set* $M = m_1 + ... + m_l$ *and denote the set of such stratified subsampling schemes by* $\Lambda(K, \lambda, m)$*.*

The constant λ is a multiplier which shrinks the batch length according to the number of samples in $\Omega \in \Lambda(K, \lambda, m)$. It has been selected empirically in the following experiments with a lower limit of $\lambda = 1$. We have also selected $m = 2$. In the following, we seek a deterministic sampling pattern that optimizes the positions of the samples within batches.

3) Optimization of the Sampling Pattern: Let $\Omega = \{s_1, s_2, ..., s_m\} \in \Lambda(K, \lambda, m)$ be a stratified sampling pattern. The pairwise distances between elements in Ω can be

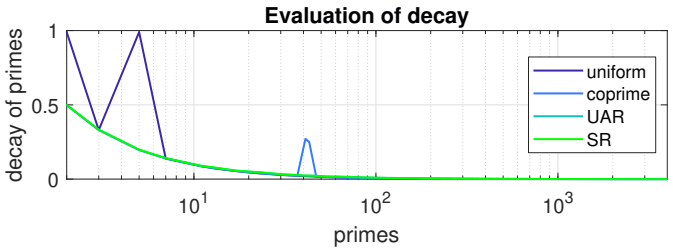

Fig. 5: Decay of multiples of primes $U_{K,m}(p)$ for pairwise distances $D_{K,m}$ for uniform sampling (*uniform*), coprime sampling (*coprime*), uniform at random sampling (*UAR*), and stratified sampling (*SR*). 5% sampling is used for $N = 4000$.

calculated as $D_{K,m} = \{d_{i,j}\}$, with $d_{i,j} = s_j - s_i$ for $j > i$. We denote this list (which includes possible repeats) as $D_{K,m} = \{d_1, ..., d_{L_D}\}$, where $L_D = m(m-1)/2$.

Let $\mathcal{P}_N = \{p_1, p_2, ..., p_{L_P}\}$ be the collection of primes smaller than N and define, for each prime $p \in \mathcal{P}_N$,

$$U_{K,m}(p) := \frac{1}{L_D} \sum_{j=1}^{L_D} \nu_j, \quad \nu_j = \begin{cases} 1 \text{ if } & d_j \mod (p) = 0 \\ 0 \text{ else.} \end{cases} \tag{4}$$

In other words, the decay of primes $U_{K,m}(p)$ tells the proportion of elements of $D_{K,m}$ that are divisible by the prime p.

The key idea is the following. If $U_{K,m}(p_i) > U_{K,m}(p_{i+1})$ and $p_{i+1} > p_i$, then subgroups of distances can be prevented; thereby, robustness of the sampling pattern and optimal reconstruction can be ensured. The motivation for this is the result of [7] that states that a signal can be reconstructed exactly from partially known Fourier coefficients $\Omega \subsetneq \mathbb{Z}_N$ if N is a prime integer. Therefore, we introduce the following quantity:

$$Dc(\Omega) := \frac{1}{L_P} \sum_{j=1}^{L_P - 1} \max \left\{ 0, \frac{U_{K,m}(p_{j+1}) - U_{K,m}(p_j)}{U_{K,m}(p_j)} \right\}. \tag{5}$$

The corresponding algorithm is shown in Algorithm 1. We then seek to solve the following optimization problem:

$$\min_{\Omega \in \Lambda(K,\lambda,m)} Dc(\Omega). \tag{6}$$

Solving such an optimization problem, i.e. constructing a deterministic stratified pattern Ω with minimum overall decay $Dc(\Omega)$, is a highly non-trivial task. We use a Monte Carlo simulation to create a large number of stratified sampling patterns and select the pattern with minimum overall decay Dc (see Algorithm 2). In the simulation, stratified patterns are created by distributing samples uniformly at random per batch. This is referred to as *stratified-random* (SR) sampling in the following. Accordingly, the optimized pattern is denoted as *stratified-random-minimized* (SRM) pattern.

As an example, the decay $Dc(\Omega)$ is analyzed for four different sampling patterns in Figure 5. In the case of UAR and SR sampling, one can note a smooth decay with $U_{K,m}(p_i) > U_{K,m}(p_{i+1})$. On the other hand, uniform sampling results in two distinct peaks at $p = 2$ and $p = 5$. Additionally, *co-prime* sampling, which has successfully been used in the field of array sensing to find the optimal placement of single

Algorithm 1 Minimize multiples in SR pattern

```
function FINDDECAY(pattern)
  N = length(pattern)
  idx = find(pattern==1)        ▷ index of sample locations
  D = [];
  for i = 1:N                   ▷ get all distances
    for j = idx(i):N
      D = [D,idx(j)-idx(i)]
    end for
  end for
  P = primes(N)                 ▷ all primes till length of pattern
  for i = 1:length(P)
    U(i) = find(D==n P(i)), n∈ ℤ   ▷ find multiples
  end for
  decay = diff(U)/U;            ▷ decay function
  Dc = sum(decay) for decay >0  ▷ overall decay
return Dc
```

Algorithm 2 Pattern creation by using Monte Carlo simulation

```
function MINIMIZEMULTIPLESSRPATTERN(K,M)
  runs = 1000                   ▷ how many patterns to test
  decayMIN = 100                ▷ initialize
  for i = 1:runs
    pattern = getPattern(K,M)   ▷ SR pattern, §III-A2
    Dc = findDecay(pattern)
    if Dc ≤ decayMIN
      patternOPT = pattern
      decayMIN = Dc
    end if
  end for
return patternOPT
```

measurements [43]–[45], is analyzed but results in an increase in multiples for the two distances $p = 41$ and $p = 43$.

4) Numerical Evaluation: In order to recover x from y, the matrix $A = P_\Omega \Psi^* P_\mathcal{S}$ must be injective. A useful quantity in this regard is the condition number $\kappa(C)$ with $C = A^*A$.

We simulate three different signal models with (i) exactly one non-zero frequency with $\mathcal{S} = \{K\}$, (ii) non-zero frequencies $k \leq K$ with $\mathcal{S} = \{1, .., K\}$ and (iii) low frequencies with two additional frequencies $\mathcal{S} = \{1, .., K, \frac{N}{4}, \frac{N}{2}\}$. The sensing matrix P_Ω is generated for UAR, SR and SRM sampling.

Results show that condition numbers are significantly smaller for SRM sampling than for UAR sampling (see Figure 6). Applying ℓ_1-reconstruction as in Equation (1) for all sampling patterns supports those findings. Figure 7 shows a worst-case scenario of SR sampling, for which reconstruction is significantly improved by using SRM sampling. An overall evaluation of sampling patterns for all three signal models demonstrates a reduction of reconstruction errors for SRM sampling in comparison to UAR sampling (see Figure 8). Consequently, our proposed SRM sampling method can be used to improve the reconstruction results of structured signals at low sampling rates.

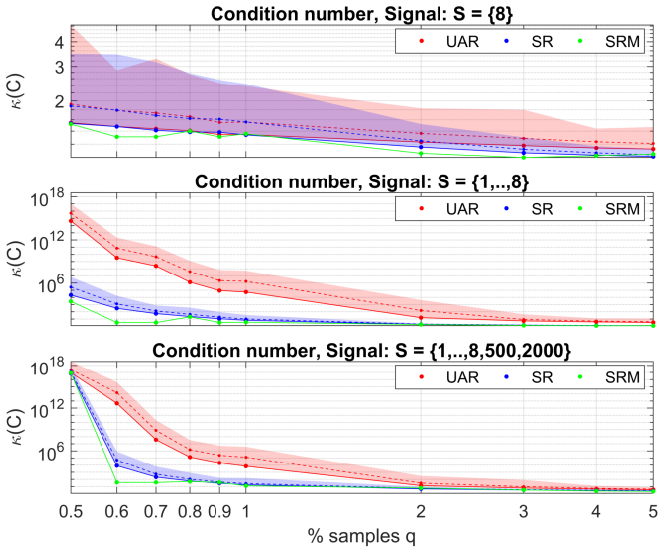

Fig. 6: Condition number $\kappa(C)$ visualized. Shaded areas, solid and dashed lines represent maximum, mean and mean with additional standard deviation of respective $\kappa(C)$ for 1000 realizations each. Results are shown for UAR, SR and SRM sampling with different percentages of samples $q = \frac{M}{N}$ and signal length $N = 1000$. The low frequency range is set to $K = 8$. Three different signal models are simulated, Top: $\mathcal{S} = \{8\}$, Middle: $\mathcal{S} = \{1, .., 8\}$, Bottom: $\mathcal{S} = \{1, .., 8, 500, 2000\}$.

5) Main Findings: Our findings on the design of a structured sampling pattern for adapting signal acquisition to the structure of the input signal can be summarized as follows:

- The direct transfer of structured sampling approaches in Fourier sensing to sensing in time or image domain is impossible. Independent of the signal structure, the sampling pattern needs to show a smooth decay of prime occurrences for optimal reconstruction.
- Signal structure can be considered by using stratified sampling, which restricts distances between adjacent samples.
- If the signal structure is dominated by the low-frequency range as occurring in many applications, SRM sampling can be used to significantly increase reconstruction accuracy.

B. Structured Reconstruction

1) Estimation of Signal Structure: While a general knowledge of the signal structure is sufficient to design a suitable sampling pattern, e.g. focusing on the recovery of low frequencies, knowledge of the location of those frequencies improves reconstruction. Several approaches have been proposed for iteratively adapting the DFT via dictionary learning [32], [33]. However, this leads to a non-uniform grid, for which a fast implementation via the FFT is impractical. Our approach focuses on a feasible implementation for real-world applications based on the FFT as an implementation of the DFT, thereby reducing computational effort and memory consumption.

The signal structure can be estimated from under-sampled measurements $y = P_\Omega x$ by optimizing the representation Y

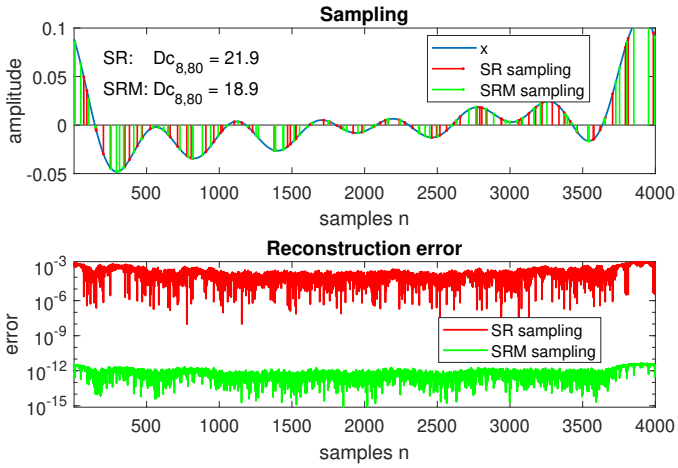

Fig. 7: Exemplary worst case scenario for SR sampling in comparison to SRM sampling. Top: Original signal with $\mathcal{S} = \{1, .., 8\}$, $N = 4000$, 2% of samples used, i.e. $M = 80$. The decay Dc is also shown. Bottom: Reconstruction error $\|x - \tilde{x}\|$ on a logarithmic scale, where $\tilde{x}$ is reconstructed by using (i) SR sampling and (ii) SRM sampling.

resulting from $Y = \Psi_{\widehat{N}} y$, where

$$(\Psi_{\widehat{N}} y)[k] = Y[k] = \sum_{n=0}^{N-1} (P_\Omega x)[n] e^{\frac{2\pi i n k}{\widehat{N}}} = \sum_{n \in \Omega} y[n] e^{\frac{2\pi i n k}{\widehat{N}}}, \tag{7}$$

with $\widehat{N} \geq N$ being the size of the DFT. Let $\epsilon > 0$ be a hard threshold and let I_1 denote the indices corresponding to coefficients of Y greater in magnitude than ϵ and I_0 be the complementary indices. For an ideal sparse representation, we expect the following sparsity measure χ to be large,

$$\chi\left(\widehat{N}\right) := \frac{\frac{1}{|I_1|} \sum_{j \in I_1} |Y_j|}{\frac{1}{|I_0|} \sum_{j \in I_0} |Y_j|}. \tag{8}$$

We can therefore select a DFT size which seeks to maximize χ over a suitable range of sizes

$$\max \chi(\widehat{N}). \tag{9}$$

In many applications, prior knowledge on the signal structure is available based on simulations, construction plans, experiments, physical, chemical or biological properties etc. and can replace or support structure estimation in Equation (9).

2) Implementation: We now discuss how to implement the optimization problem with regard to the DFT size $\widehat{N}$. The optimization problem can be interpreted in two different ways: (i) If $\widehat{N} = cN$ with $c \in \mathbb{N}$, the optimization problem corresponds to c-fold subsampling. Subsampling can be used to adapt the DFT to the signal structure but is only successful if a large c is chosen. However, this comes along with increased computational effort and storage consumption while decreasing sparsity. Therefore, subsampling should not be used as a method on its own but can be used to complement structure estimation.

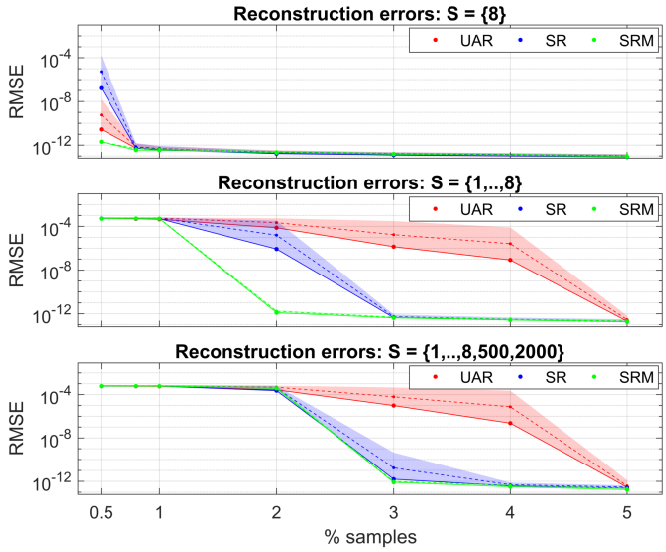

Fig. 8: Comparison of reconstruction results for UAR, SR and SRM sampling and different percentages of samples $q = \frac{M}{N}$, $N = 4000$. Solid lines, dashed lines and shaded areas represent the mean, the mean plus standard deviation and the maximum of root-mean-square errors (RMSE) in the time domain for 1000 realizations each. The three signal models are the same as described in Figure 6.

(ii) If $\widehat{N} = \theta^{-1}N$ with $\theta^{-1} \in (1, 2)$, the optimization problem corresponds to stretching of the fixed grid of the DFT by a factor θ:

$$\sum_{n\in\Omega} x[n]e^{\frac{2\pi i n k}{\widehat{N}}} = \sum_{n\in\Omega} x[n]e^{2\pi i\theta\frac{k}{N}n}. \tag{10}$$

In case of a harmonic signal model, i.e. $\mathcal{S} = \{f_0, 2f_0, 3f_0, ...\}$, the size of the DFT can be estimated as

$$\widehat{N} = \left\lceil \frac{f_s}{\hat{f}_0} \left\lceil Nc\frac{\hat{f}_0}{f_s} \right\rceil \right\rceil \tag{11}$$

with f_s, $\hat{f}_0$ being the sampling frequency and the estimated fundamental frequency, respectively.

(iii) A combination of stretching and subsampling can be implemented by selecting $cN < \widehat{N} < (c+1)N$ for $c \in \mathbb{N}$, e.g. to account for a harmonic signal model with a small number of higher non-harmonics, such as $\mathcal{S} = \{f_0, 2f_0, 3f_0, f_{i1}, f_{i2}\}$.

Simulation results in Figure 9 show that reconstruction errors can significantly be reduced by both stretching and subsampling. Lowest reconstruction errors are achieved by combining the two methods of bin stretching and subsampling. In doing so, grid mismatch is reduced for harmonics by grid stretching and for non-harmonics by subsampling. The computational effort remains small due to using the FFT.

3) Main Findings:

- The signal structure can be estimated by maximizing a sparsity measure. Estimation can be complemented by prior knowledge in many applications.
- Window and grid mismatch can be addressed by adapting the representation matrix Ψ to the model of the signal by using a combination of stretching and subsampling.

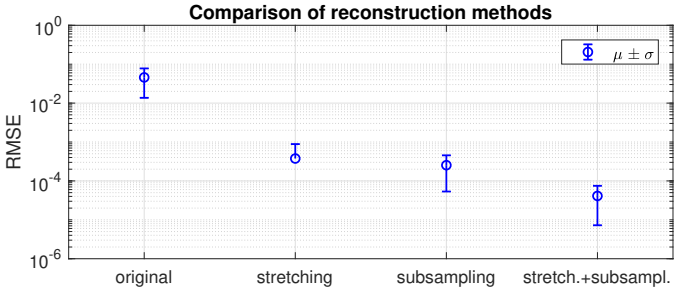

Fig. 9: Reconstruction results for *original* ($c = 1$), *stretching* ($1 \leq c < 2$), *subsampling* ($c = 3$) , *strech.+subsampl.* ($3 \leq c < 4$) for an input signal of length $N = 4000$ and size of DFT $\widehat{N} = cN$. If c comprises a range, the $\widehat{N}$ maximizing χ is picked. The input signal consists of $\{f_0, 2f_0, 3f_0, f_i, f_j\}$ with randomly selected $0.1 \leq f_0 \leq 0.2$ Hz and $10 \leq f_i, f_j \leq 20$ Hz. Reconstruction computed for 10% of samples, SRM sampling with low frequency range $K = 10$ used. Mean μ and standard deviation σ of root-mean-square errors (RMSE) displayed.

- To keep computational effort at bay, the FFT is used to compute Ψ. The number of frequency points is moderately increased up to the best match of estimated signal model and frequency grid.

IV. Applications

In the following, our findings are demonstrated by means of two applications. First, structured CS is applied to the emerging field of SHM, in which measurements are conducted in the time domain (§IV-A). Second, structure is incorporated into CS of EM images which are acquired using time- and image-domain-based sensing (§IV-B).

A. Structural Health Monitoring

In the field of SHM, sensor networks are widely used to continuously monitor the condition of civil structures. Since sensors often operate wirelessly and depend on energy harvesting methods, CS is promising to reduce the energy needed for measurements as well as for wireless data transmission [35]–[37]. Even though vibration measurements in SHM applications are highly structured, signal structure is still being neglected in the vast majority of CS approaches.

In our example, we focus on CS in the field of wind turbines, in which continuous monitoring is essential to increase the safety and competitiveness of wind energy. By measuring vibrations of the turbine blades, blade damage can be detected and turbine settings can be optimized to reduce load and forces acting on the blades [46], [47].

The vibrational response of a turbine blade was measured in operation of the turbine by mounting triaxial accelerometers on the blade tip as described in [48]. To reduce the impact of noise at high rotation frequencies, only measurements at low rotation frequencies ($f_0 \leq 0.15$ Hz) were evaluated. Also, the following analysis is based on measurements in x-direction of the sensor, which experienced the lowest noise levels. Acceleration was measured at 400 Hz for a duration of 10 s. The sampling matrix has not been integrated into

Fig. 10: Original and reconstructed acceleration, 10% of samples used. Comparison of (i) traditional CS (UAR sampling and reconstruction with original resolution, $\hat{N} = N$) and (ii) structured CS (SRM sampling for a low frequency range of $K = 10$ and reconstruction with stretching and threefold subsampling, $3N \leq \hat{N} \leq 4N$).

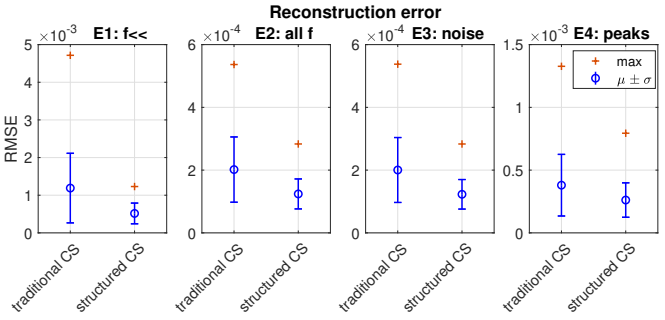

Fig. 11: Reconstruction errors for 100 acceleration measurement campaigns. Comparison of (i) traditional CS (UAR sampling, reconstruction with original resolution, $\hat{N} = N$) and (ii) structured CS (SRM sampling for a low frequency range of $K = 10$ and reconstruction with stretching and threefold subsampling, $3N \leq \hat{N} \leq 4N$). 10% of samples are used and the mean μ, standard deviation σ and maximum of root-mean-square errors (RMSE) are displayed.

the prototype sensor yet; therefore, compressed measurements are simulated and are selected from the set of measurements according to the sampling matrix.

Figure 10 shows original and reconstructed acceleration for traditional CS and structured CS where 10% of samples are used for both sampling methods. One can clearly note that the measured signal is dominated by the fundamental rotation frequency, which does not coincide with the measurement window. Consequently, *window mismatch* and resulting *grid mismatch* lead to poor reconstruction results for traditional CS. When using structured CS instead, the fundamental frequency is incorporated into reconstruction and, thereby, reconstruction accuracy at the boundaries of the measurement interval is improved significantly.

Next, the overall reconstruction accuracy is evaluated by calculating the following errors in the frequency domain:

E1: Low-frequency error for $k \leq 10$ in the frequency domain.
E2: Overall error across all frequencies.
E3: Noise error: Distinct peaks in the original spectrum are identified. The error is then computed for all remaining frequencies to assess the number of falsely created peaks.
E4: Peak error for the 10 peaks with largest amplitude.

Results for 100 measurement campaigns are depicted in

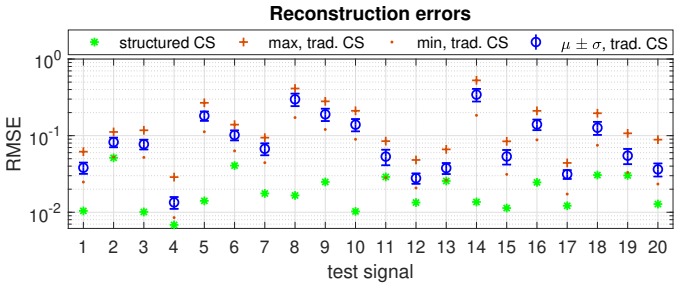

Fig. 12: Variability of reconstruction errors for traditional CS (UAR sampling, reconstruction with $\hat{N} = N$) in comparison to structured CS (fixed SRM sampling, structured reconstruction with $N \leq \hat{N} \leq 3N$). 20 one-dimensional images simulated (piecewise linear functions, signal length $N = 4000$) with 100 UAR patterns tested per image. 5% of samples used and root-mean-square errors (RMSE) displayed.

Figure 11. Reconstruction errors for all error measures are reduced by using structured CS. To summarize, incorporating the signal structure into CS algorithms is beneficial in SHM applications such as monitoring of wind turbine blades.

B. 2D Imaging

CS is promising in imaging methods such as electron microscopy (EM), in which samples are acquired according to fixed positions in the image domain. By reducing the number of measurements, the risk of damaging sensitive structures can be reduced. Different variants of EM have incorporated CS methods, such as fluorescence microscopy [49], atomic force microscopy [50], random-beam scanning transmission EM [51] and scanning line probe imaging [52]. Even though the implementation of the sensing matrix was optimized and adapted in a few approaches [50], [53], no specific attention has been paid to the design of the sensing matrix itself.

In the following, two experiments are performed for evaluating the benefit of structured CS for EM.

1) Experiment 1 - 1D Evaluation of structured CS: First, the variability of UAR sampling in traditional CS is evaluated against fixed SRM sampling in structured CS. To reduce computational complexity, one-dimensional (1D) test signals are created by using piecewise linear functions and 100 UAR patterns are tested per signal. Results show that reconstruction errors for structured CS are smaller than for traditional CS for all test signals (see Figure 12). Additionally, errors for traditional CS are highly variable both within and between test signals, with the maximum error of structured CS being 10 times smaller than the maximum error of traditional CS.

2) Experiment 2 - 2D Test images: Next, the benefit of structured CS in EM is evaluated. When moving from 1D to 2D test signals, the design of the sampling matrix needs to be extended to two dimensions. For this, the concept of 1D batches in stratified subsampling is extended to 2D batches and the pairwise distance between elements in Ω are calculated as Euclidean distances $d_{i,j} = (d_i^2 + d_j^2)^{\frac{1}{2}}$. In addition, the signal structure is estimated by adapting the size $[\hat{N}_1, \hat{N}_2]$ of the two-dimensional DFT.

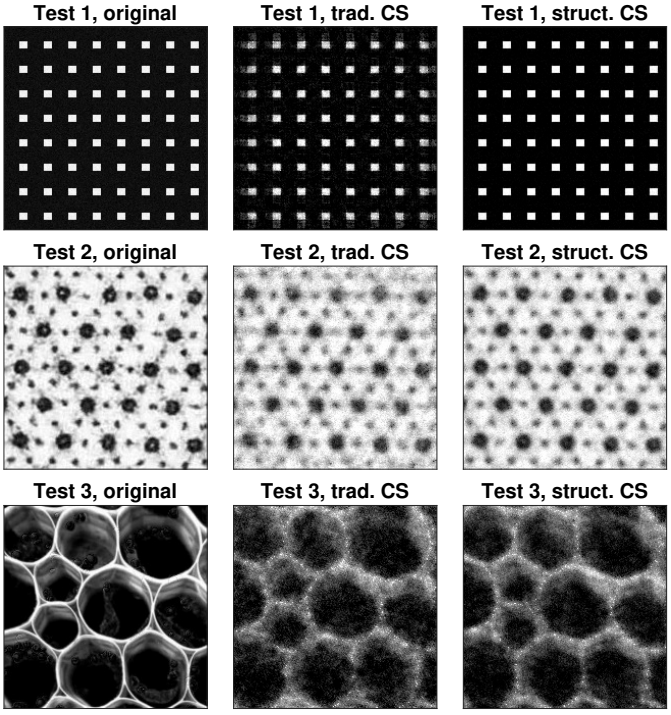

Fig. 13: Image reconstruction by using traditional CS, i.e. UAR sampling, and structured CS, i.e. SRM sampling designed for $K = 10$ and structured reconstruction with $3N \leq \hat{N} \leq 4N$. 10% samples used. From left to right: (i) original images of size 200 x 200, (ii) traditional CS and (iii) structured CS reconstruction. Top row: test image with 2% noise, relative L2 error 0.36 / 0.10 and PSNR $19.2\,\mathrm{dB}$ / $30.2\,\mathrm{dB}$ for traditional and structured CS, respectively. Middle row: EM image of animal cells, snippet from [54], rel. L2 error 0.16 / 0.13 and PSNR $17.5\,\mathrm{dB}$ / $19.3\,\mathrm{dB}$. Bottom row: EM image of animal cells, snippet from [55], rel. L2 error 0.47 / 0.42 and PSNR $15.1\,\mathrm{dB}$ / $16.1\,\mathrm{dB}$.

In order to demonstrate our method, one highly structured test image and two EM images of animal cells are tested (see Figure 13). For the test image (Image 1), reconstruction accuracy can be increased significantly by 71.3%. Also, the peak signal-to-noise ratio (PSNR) can be increased significantly by $11.0\,\mathrm{dB}$. For the real-world EM images, structure is not as prominent as for the 1D SHM application. Consequently, reconstruction accuracy is increased by 15.6% and 9.3%, and PSNRs are increased by $1.8\,\mathrm{dB}$ and $1.0\,\mathrm{dB}$ for Image 2 and Image 3, respectively, by using structured CS.

As for the 1D case, structured CS is expected to increase robustness but either needs computationally costly Monte Carlo simulations or profound mathematical elaboration to be verified. This exceeds the scope of this paper and will be covered in future work. One needs to note that in our applications images are sampled by picking single locations as needed in EM. This is a different task than in many image reconstruction problems, in which Fourier sensing is paired with reconstruction by using wavelets. Therefore, results can not be compared to those reconstruction problems one-by-one.

V. Conclusion

Even though structured CS is state-of-the-art in Fourier sensing applications, structure is still neglected in most time- and image-domain-based sensing applications. In this paper, we developed a method to incorporate structure into both the acquisition of samples and the reconstruction of signals, thereby significantly reducing reconstruction errors in such applications. The sensing matrix was designed via stratified random sampling with the sample intervals being related to the largest frequency being captured. Also, a measure for optimizing the sampling pattern was proposed to increase the robustness of reconstruction. Additionally, we propose structured reconstruction for reducing grid mismatch of the Fourier transform while keeping computational costs low.

Simulation results show that structured CS significantly reduces reconstruction errors and increases robustness. Structured CS also successfully reduces reconstruction errors in an SHM application. Error reduction was smaller in 2D EM and we propose further research on the estimation of signal structure in 2D images in the future. Our approach represents first steps from structured Fourier sensing to time- and image-domain-based sensing, and we hope that it will initiate further work on structured sampling and how it can be generalized.

Acknowledgments

This work was supported by the Austrian Research Promotion Agency FFG, Research Partnerships - 862437, and the company eologix sensor technology (T.L), a Research Fellowship at Trinity College, Cambridge (M.J.C.), a Leverhulme Prize and a Royal Society University Research Fellowship (A.C.H.). T.L. wishes to thank the Department of Applied Mathematics and Theoretical Physics, University of Cambridge, for hosting a research stay during which work for this paper took place.

References

[1] G. Anastasi, M. Conti, M. Di Francesco, and A. Passarella, "Energy conservation in wireless sensor networks: A survey," *Ad Hoc Networks*, vol. 7, no. 3, pp. 537 – 568, 2009.

[2] R. Evans, S. Taylor, S. Janes, S. Halligan, A. Morton, N. Navani, A. Oliver, A. Rockall, J. Teague, and A. Miles, "Patient experience and perceived acceptability of whole-body magnetic resonance imaging for staging colorectal and lung cancer compared with current staging scans: A qualitative study," *BMJ open*, vol. 7, no. 9, 2017.

[3] D. Nicholls, J. Lee, H. Amari, A. J. Stevens, B. L. Mehdi, and N. D. Browning, "Minimising damage in high resolution scanning transmission electron microscope images of nanoscale structures and processes," *Nanoscale*, vol. 12, no. 41, pp. 21 248–21 254, 2020.

[4] E. J. Candès *et al.*, "Compressive sampling," in *Proceedings of the International Congress of Mathematicians*, vol. 3. Madrid, Spain, 2006, pp. 1433–1452.

[5] M. Rani, S. Dhok, and R. Deshmukh, "A systematic review of compressive sensing: Concepts, implementations and applications," *IEEE Access*, vol. 6, pp. 4875–4894, 2018.

[6] D. L. Donoho, "Compressed sensing," *IEEE Transactions on information theory*, vol. 52, no. 4, pp. 1289–1306, 2006.

[7] E. J. Candès, J. Romberg, and T. Tao, "Robust uncertainty principles: Exact signal reconstruction from highly incomplete frequency information," *IEEE Transactions on Information Theory*, vol. 52, no. 2, pp. 489–509, 2006.

[8] Y. Bao, Z. Tang, and H. Li, "Compressive-sensing data reconstruction for structural health monitoring: A machine-learning approach," *Structural Health Monitoring*, p. 1475921719844039, 2019.

[9] D. Zhao, F. Zhao, and Y. Gan, "Reference-driven compressed sensing MR image reconstruction using deep convolutional neural networks without pre-training," *Sensors*, vol. 20, no. 1, p. 308, 2020.

[10] V. Antun, M. J. Colbrook, and A. C. Hansen, "Can stable and accurate neural networks be computed? - On the barriers of deep learning and Smale's 18th problem," *arXiv preprint arXiv:2101.08286*, 2021.

[11] C. Szegedy, W. Zaremba, I. Sutskever, J. Bruna, D. Erhan, I. J. Goodfellow, and R. Fergus, "Intriguing properties of neural networks," in *Int. Conf. on Learning Representations*, 2014.

[12] S.-M. Moosavi-Dezfooli, A. Fawzi, and P. Frossard, "Deepfool: a simple and accurate method to fool deep neural networks," in *Proceedings of the IEEE Conference on Computer Vision and Pattern Recognition*, 2016, pp. 2574–2582.

[13] N. Akhtar and A. Mian, "Threat of adversarial attacks on deep learning in computer vision: A survey," *IEEE Access*, vol. 6, pp. 14 410–14 430, 2018.

[14] N. Carlini and D. Wagner, "Audio adversarial examples: Targeted attacks on speech-to-text," in *2018 IEEE Security and Privacy Workshops (SPW)*. IEEE, 2018, pp. 1–7.

[15] Y. Huang, T. Würfl, K. Breininger, L. Liu, G. Lauritsch, and A. Maier, "Some investigations on robustness of deep learning in limited angle tomography," in *International Conference on Medical Image Computing and Computer-Assisted Intervention*. Springer, 2018, pp. 145–153.

[16] V. Antun, F. Renna, C. Poon, B. Adcock, and A. C. Hansen, "On instabilities of deep learning in image reconstruction and the potential costs of AI," *Proceedings of the National Academy of Sciences*, vol. 117, no. 48, pp. 30 088–30 095, 2020.

[17] S. G. Finlayson, J. D. Bowers, J. Ito, J. L. Zittrain, A. L. Beam, and I. S. Kohane, "Adversarial attacks on medical machine learning," *Science*, vol. 363, no. 6433, pp. 1287–1289, 2019.

[18] F. Knoll, T. Murrell, A. Sriram, N. Yakubova, J. Zbontar, M. Rabbat, A. Defazio, M. J. Muckley, D. K. Sodickson, C. L. Zitnick, and M. P. Recht, "Advancing machine learning for MR image reconstruction with an open competition: Overview of the 2019 fastMRI challenge," *Magnetic Resonance in Medicine*, 2020.

[19] M. J. Muckley, B. Riemenschneider, A. Radmanesh, S. Kim, G. Jeong, J. Ko, Y. Jun, H. Shin, D. Hwang, M. Mostapha *et al.*, "State-of-the-art Machine Learning MRI Reconstruction in 2020: Results of the Second fastMRI Challenge," *arXiv preprint arXiv:2012.06318*, 2020.

[20] B. Adcock, A. C. Hansen, C. Poon, and B. Roman, "Breaking the coherence barrier: A new theory for compressed sensing," in *Forum of Mathematics, Sigma*, vol. 5. Cambridge University Press, 2017.

[21] C. Boyer, J. Bigot, and P. Weiss, "Compressed sensing with structured sparsity and structured acquisition," *Applied and Computational Harmonic Analysis*, vol. 46, no. 2, pp. 312–350, 2019.

[22] Y. Traonmilin and R. Gribonval, "Stable recovery of low-dimensional cones in Hilbert spaces: One RIP to rule them all," *Applied and Computational Harmonic Analysis*, vol. 45, no. 1, pp. 170–205, 2018.

[23] A. Bastounis and A. C. Hansen, "On the absence of the rip in real-world applications of compressed sensing and the rip in levels," *arXiv preprint arXiv:1411.4449*, 2014.

[24] B. Adcock and A. C. Hansen, "Generalized sampling and infinite-dimensional compressed sensing," *Foundations of Computational Mathematics*, vol. 16, no. 5, pp. 1263–1323, 2016.

[25] C. Li and B. Adcock, "Compressed sensing with local structure: uniform recovery guarantees for the sparsity in levels class," *Applied and Computational Harmonic Analysis*, vol. 46, no. 3, pp. 453–477, 2019.

[26] C. Boyer, J. Bigot, and P. Weiss, "Compressed sensing with structured sparsity and structured acquisition," *Applied and Computational Harmonic Analysis*, vol. 46, no. 2, pp. 312–350, 2019.

[27] Y. C. Eldar, P. Kuppinger, and H. Bolcskei, "Block-sparse signals: Uncertainty relations and efficient recovery," *IEEE Transactions on Signal Processing*, vol. 58, no. 6, pp. 3042–3054, 2010.

[28] B. Adcock, S. Brugiapaglia, and M. King-Roskamp, "Iterative and greedy algorithms for the sparsity in levels model in compressed sensing," in *Wavelets and Sparsity XVIII*, vol. 11138. International Society for Optics and Photonics, 2019, p. 1113809.

[29] L. Feng, T. Benkert, K. T. Block, D. K. Sodickson, R. Otazo, and H. Chandarana, "Compressed sensing for body MRI," *Journal of Magnetic Resonance Imaging*, vol. 45, no. 4, pp. 966–987, 2017.

[30] M. F. Duarte and Y. C. Eldar, "Structured compressed sensing: From theory to applications," *IEEE Transactions on Signal Processing*, vol. 59, no. 9, pp. 4053–4085, 2011.

[31] Y. Chi, L. L. Scharf, A. Pezeshki, and A. R. Calderbank, "Sensitivity to basis mismatch in compressed sensing," *IEEE Transactions on Signal Processing*, vol. 59, no. 5, pp. 2182–2195, 2011.

[32] J. Fang, F. Wang, Y. Shen, H. Li, and R. S. Blum, "Super-resolution compressed sensing for line spectral estimation: An iterative reweighted approach," *IEEE Transactions on Signal Processing*, vol. 64, no. 18, pp. 4649–4662, 2016.

[33] L. Hu, Z. Shi, J. Zhou, and Q. Fu, "Compressed sensing of complex sinusoids: An approach based on dictionary refinement," *IEEE Transactions on Signal Processing*, vol. 60, no. 7, pp. 3809–3822, 2012.

[34] S. Bernhardt, R. Boyer, S. Marcos, and P. Larzabal, "Compressed sensing with basis mismatch: Performance bounds and sparse-based estimator," *IEEE Transactions on Signal Processing*, vol. 64, no. 13, pp. 3483–3494, 2016.

[35] D. Mascareñas, A. Cattaneo, J. Theiler, and C. Farrar, "Compressed sensing techniques for detecting damage in structures," *Structural Health Monitoring*, vol. 12, no. 4, pp. 325–338, 2013.

[36] Y. Yang and S. Nagarajaiah, "Output-only modal identification by compressed sensing: Non-uniform low-rate random sampling," *Mechanical Systems and Signal Processing*, vol. 56, pp. 15–34, 2015.

[37] Y. Bao, Z. Shi, X. Wang, and H. Li, "Compressive sensing of wireless sensors based on group sparse optimization for structural health monitoring," *Structural Health Monitoring*, vol. 17, no. 4, pp. 823–836, 2018.

[38] C. S. Hansel, M. N. Holme, S. Gopal, and M. M. Stevens, "Advances in high-resolution microscopy for the study of intracellular interactions with biomaterials," *Biomaterials*, p. 119406, 2019.

[39] S. Thomas, R. Thomas, A. K. Zachariah, and R. Kumar, *Microscopy methods in nanomaterials characterization*. Elsevier, 2017, vol. 1.

[40] P. Binev, W. Dahmen, R. DeVore, P. Lamby, D. Savu, and R. Sharpley, "Compressed sensing and electron microscopy," in *Modeling Nanoscale Imaging in Electron Microscopy*. Springer, 2012, pp. 73–126.

[41] E. J. Candès and M. B. Wakin, "An introduction to compressive sampling [a sensing/sampling paradigm that goes against the common knowledge in data acquisition]," *IEEE Signal Processing Magazine*, vol. 25, no. 2, pp. 21–30, 2008.

[42] H. Nyquist, "Certain topics in telegraph transmission theory," *Transactions of the American Institute of Electrical Engineers*, vol. 47, no. 2, pp. 617–644, 1928.

[43] P. Pal and P. P. Vaidyanathan, "Coprime sampling and the music algorithm," in *2011 Digital Signal Processing and Signal Processing Education Meeting (DSP/SPE)*. IEEE, 2011, pp. 289–294.

[44] A. Koochakzadeh and P. Pal, "On the robustness of co-prime sampling," in *2015 23rd European Signal Processing Conference (EUSIPCO)*. IEEE, 2015, pp. 2825–2829.

[45] T. Jia, H. Wang, X. Shen, and X. Liu, "Direction of arrival estimation with co-prime arrays via compressed sensing methods," in *OCEANS 2016-Shanghai*. IEEE, 2016, pp. 1–5.

[46] D. Tcherniak and L. L. Mølgaard, "Active vibration-based structural health monitoring system for wind turbine blade: Demonstration on an operating vestas V27 wind turbine," *Structural Health Monitoring*, vol. 16, no. 5, pp. 536–550, 2017.

[47] Y. Du, S. Zhou, X. Jing, Y. Peng, H. Wu, and N. Kwok, "Damage detection techniques for wind turbine blades: A review," *Mechanical Systems and Signal Processing*, vol. 141, p. 106445, 2020.

[48] T. Loss, O. Gerler, and A. Bergmann, "Online calibration of accelerometers for monitoring of wind turbine blade movement," in *2020 IEEE International Instrumentation and Measurement Technology Conference (I2MTC)*. IEEE, 2020.

[49] V. Studer, J. Bobin, M. Chahid, H. S. Mousavi, E. Candes, and M. Dahan, "Compressive fluorescence microscopy for biological and hyperspectral imaging," *Proceedings of the National Academy of Sciences*, vol. 109, no. 26, pp. E1679–E1687, 2012.

[50] C. S. Oxvig, T. Arildsen, and T. Larsen, "Structure assisted compressed sensing reconstruction of undersampled afm images," *Ultramicroscopy*, vol. 172, pp. 1–9, 2017.

[51] L. Donati, M. Nilchian, S. Trépout, C. Messaoudi, S. Marco, and M. Unser, "Compressed sensing for STEM tomography," *Ultramicroscopy*, vol. 179, pp. 47–56, 2017.

[52] H.-W. Kuo, A. E. Dorfi, D. V. Esposito, and J. N. Wright, "Compressed sensing microscopy with scanning line probes," *arXiv preprint arXiv:1909.12342*, 2019.

[53] X. Liu, S. Zhang, A. Yurtsever, and J. Liang, "Single-shot real-time sub-nanosecond electron imaging aided by compressed sensing: Analytical modeling and simulation," *Micron*, vol. 117, pp. 47–54, 2019.

[54] J. A. Don W. Fawcett, "Cil_36063, bombylius major, flight muscle cell," 2011. [Online]. Available: http://www.cellimagelibrary.org/images/36063, accessed 2021-01-08

[55] M. Guervos, "Cil_40405, convallaria majalis," 2012. [Online]. Available: http://www.cellimagelibrary.org/images/40405, accessed 2021-01-08